JJMIE

Volume 11 Number 2, April. 2017
ISSN 1995-6665
Pages 73 -78

Jordan Journal of Mechanical and Industrial Engineering

Pinning Effect of Pores on Grain Growth in Sintered Steel

Nathir A. Rawashdeh [*a], Walid Khraisat [b], Henrik Borgström [c]

[a] Mechatronics Engineering Department, German Jordanian University, 11180 Amman, Jordan
[b] Industrial Engineering Department , The University of Jordan, 11942 Amman, Jordan
[c] Materials, Process & Products, Swerea SWECAST, Jönköping, Sweden

Received Jan., 25, 2017 Accepted Oct., 13, 2017

Abstract

The effect of pore drag on grain growth is one of the most frequent effects encountered in the last stage of sintering. Therefore, the understanding of the effect of microstructure and pore location, pore morphology on grain growth is essential. Here a migrating grain boundary interacts with pores and other grain boundaries such that its structure and energy vary during grain growth. Consequently, it is of great interest to see whether the grain boundary energy decreases or increases during the interaction between migrating grain boundaries and pores. In this paper, the conditions for grain boundary migration and pinning are related to pore curvature and illustrated theoretically and experimentally.

Keywords: *pore rounding, pore drag, grain growth, grain boundaries.*

1. Introduction

The mechanical properties of P/M materials are directly related to their microstructure and to the porosity, pores dimension, distribution, and morphology. Densification by pore elimination and grain coarsening occur simultaneously during sintering [1,2]. In the intermediate stage of sintering, pores shrink and in the last stage, grains grow to reduce the total surface and grain boundary energy [3]. Here grain boundaries with pores are a result of the misfit between particles. These pores may either retard grain growth, be separated from the grain boundaries, or move along with the grain boundaries [4]. Pores at grain boundaries, as well as triple junctions, act as pinning points that exert Zener drag on the moving grain boundaries, hence lowering the grain growth rate or leading to grain growth stagnation [4, 5, 6].

In essence, pores on the grain boundaries prevent their migration and inhibit grain growth up to a sinter density of 90 pct of the theoretical density [7]. Thereafter, the number of pores decreases and cannot hinder grain boundary migration causing rapid grain growth.

In sintering, pores shrink and change their shape by rounding off their sharp edges and develop facets as vacancies diffuse away from the pores to sinks like grain boundaries. The morphology of pores at grain boundaries are characterized by a lenticular shape, and pores within the grains are characterized by a spherical shape [8]. This occurs during the intermediate stage of sintering where the pores become smoother [9].

The presence of different curvatures inside a single pore activates the diffusion of vacancies. Therefore, smoothening off the irregularities in the same pore. So, the rounding of pores is controlled by the diffusion of vacancies [10, 11]. The vacancies concentration gradient set up by local variation of curvature activates the diffusion of vacancies [12]. Accordingly, where the surface is convexly curved, a lower vacancy concentration is found compared to concavely curved parts of the surface [8].

Most sintering models assume that accelerated grain growth occurs during the final stage of sintering and that the pore drag effect retards grain growth as long as the pores are attached to the boundary. From these models, the mechanisms controlling grain growth by pores are explained by four behaviours.

Firstly, reduced pore mobility *Mp* where pore drag controls grain growth. This is done by reducing either the diffusion coefficients of surface diffusion *Ds* and the vapor phase diffusion coefficient *Dv*, or the diffusion coefficient of lattice diffusion D_L [13]. The mobility of pores during the last stage of sintering is lower than the mobility of grains [14, 15]. If grain boundary migration is fast, pores detach from the grain boundaries. Once free from the pores the grain boundaries grow faster and consequently the pore detachment leads to a porous, *i.e.* coarse grained material [16].

Secondly, the drag effect of the pores which are quantified by considering a force balance at the pore surface. Provided that the free surface energies are isotropic, the theoretical shape of pores located at symmetric three-grains junctions is dependent on the dihedral angle as seen from Fig. 1.

* Corresponding author e-mail: nathir.rawashdeh@gju.edu.jo.

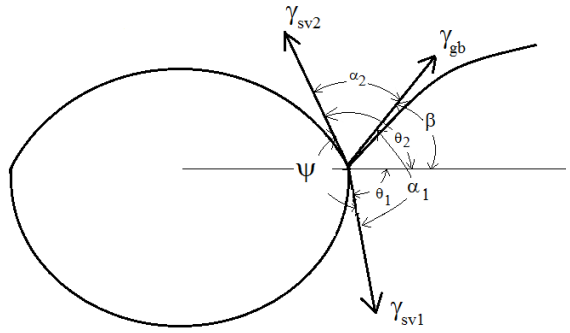

Figure1. Schematic illustration of dihedral angle ψ for solid-pore interaction adapted from [17, 18, 19, 20].

High dihedral angles mean that the grain boundary energy is low and that these grains are more likely to abnormally grow [17, 18, 21]. An increase in the dihedral angle produces an increase in the grain boundary area. The balance of force at the intersection point of the grain boundary and the pore is governed by the equation:

$$\gamma_{gb}\cos\beta = \gamma_{sv}\cos\theta_1 + \gamma_{sv}\cos\theta_2 \quad (1)$$

Though these models provide insight on pore drag and pore grain separation, the main common assumption made in these models is that: 1- the pores are of spherical morphology; 2- the angles between the surface tensions for both the trailing and the advanced parts of the pore and the grain boundary energy are equal $\alpha_1=\alpha_2$. This leads to a simplified formula for the drag force the pore exerts on the grain boundary as follows:

$$F = 2\pi r\gamma_{sv}\cos\beta\cos(\alpha-\beta) \quad (2)$$

Thirdly, the surface tension for both the trailing and the advanced part of the pore are equal. Lastly, there have been no attempts to incorporate the torque term in the force balance at the intersection point.

The primary aim of this work is to prove that detachment of pores from grain boundaries is only possible when the pore's two parts, the trailing and the advanced part, have the same radius of curvature. This work will give an attempt by using Gibbsian interfacial thermodynamics and experimental results to prove that grain boundary detachment from pores is only possible with pore spherodizing, which results from pore rounding due to surface diffusion. Thermodynamics of interfaces will be used without ignoring the effects of surface curvature.

2. Materials

The iron base powders used in experiments were ASC100 and ASC300 provided by Höganäs AB. Their maximum particle sizes are 150 µm and 45 µm, respectively, with an apparent density 3.0 g/cm^3. Three types of liquid forming additives from Höganäs AB were added to these base powders to generate a liquid phase at sintering temperature. They are pre-alloyed Fe-P-C, Fe-P-C-Mn and Fe-P-C-Cu powders produced by water atomisation. These liquid forming additives are named *LP1*, *LP2*, and *LP3* and they have P/C weight fraction ratios of 7.5, 9.33 and 8.88, respectively. Varying amounts of the liquid forming additives were mixed with the base powders to yield different fractions of liquid phases at the sintering temperature. To study the pore structure after sintering, three samples were prepared from mixing three different additives in various amounts to the base powders in order to achieve the highest possible sintered density. The compositions of the additives are shown in Table 1.

Table 1. Composition of the three samples

Samples	% C	% P	% Mn	% Cu
1	0.32	2.44	0	0
2	1.35	1.35	0	1.3
3	0.47	0.27	0	0.26

Sintering was done in N2 at 1120 °C or 1150 °C for two hours. Experiments were performed with two different heating rates of 5 and 20 °C/min.

Sample1 is made of a 30g powder mixture having a cylindrical cross section of 20mm diameter. The sample was sintered at 1120°C for two hours. This sample had a sinter density of around 98% and was subjected to long annealing at 1000 °C for 24 hours to develop the dihedral angles between pores and grain boundaries. At least 200 dihedral angles were measured for each material to obtain a statistical distribution. The heat treatment was carried out for 24 hours at 1000 °C. The atmosphere was pure N2 and the samples were cooled in air. If the *Tm* is taken as the melting temperature of pure Fe then the holding temperature for the heat treatment at 1000 °C is in the high temperature range > 0.5*Tm*. This was done to promote solid phase sintering and to dissolve the Fe_3P.

Sample 2 was double sintered first at 970 °C followed by decarburization then heated up to 1350 °C for 5 minutes. Decarburisation heat treatment was carried out in a tube furnace sealed from both ends with a reducing wet gas mixture (90%N2–10%H2). The moisture content of the atmosphere was increased by letting this gas mixture through a water container at room temperature prior to entering the furnace.

Sample3 had a rectangular cross-section of 6x6 mm^2 and was produced with different chemical compositions from powder blends of iron base powder 80% (ASC300), water-atomised liquid forming master alloy powder 10% (2.7wt% P, 2.7wt% C and 2.6wt% Cu), 0.2% graphite and lubricant addition of 0.8 wt-% H-wax. The sample was manufactured by means of single stage die compaction at 500 MPa. The green density of the die pressed sample is 83 %. After sintering, the sample was decarburised in a tube furnace starting with a gas mixture of 10% H2 and 90% N2 during heating of the sample. Then, at a temperature of 1100 °C, the moisture content of the atmosphere was increased by letting this gas mixture through a water container at room temperature prior to the furnace while heating continued at the rate of 5 °C/min to 1200 ºC with a final holding time of 120 minutes.

3. Results

Fig.2a and Fig.2b show the resulting fracture surfaces of sample 1 after being heat treated. Irregular and spherical pores at the grain boundaries are observed and no internal pores were present.

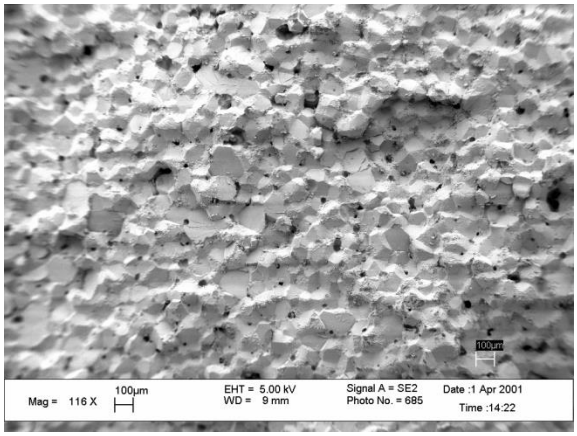

Figure 2a. Fracture surface of a Sample1 after being heat treated showing areas of porosity as well as a brittle fracture mode. The grain boundaries have no curvature.

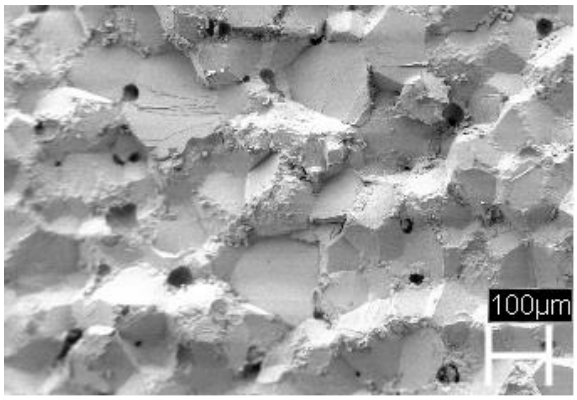

Figure 2b. Fracture surface of a Sample1 after being heat treated showing areas of porosity as well as brittle fracture mode.

Fig.3 shows the microstructure of Sample2 after final stage sintering at 1350°C for 5 minutes showing a ferritic structure surrounded by rounded pores at boundaries and the interior. Sample2 was decarburized at around 970°C for complete removal of carbon.

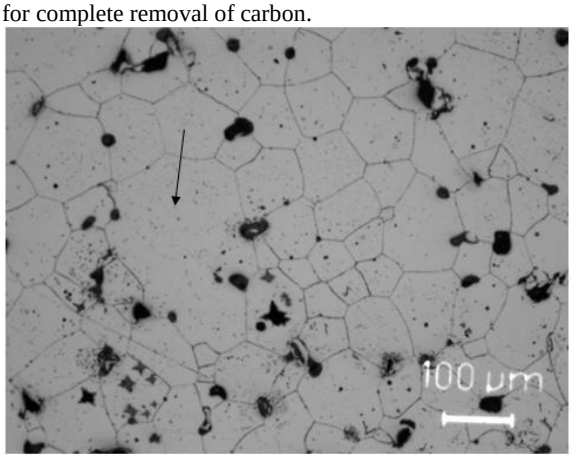

Figure 3. Microstructure of Sample2 after final stage sintering at 1350°C for 5 minutes showing ferritic structure surrounded by pores. Depicting a large, 14-sided grain.

The micrographs of Fig.1 and Fig.2 clearly show a good degree of sintering in terms of pore rounding and sinter bonding of the iron particles. Fig.3 shows the microstructure of Sample3 after decarburization. The pore morphology is not rounded as in Sample1 and Sample2. Rather, the pores' morphologies are equiaxed and the segment of the grain boundaries at the intersection points with the pores are straight. The pores are mainly concentrated at grain-particle boundaries having an irregular crack like morphology.

The morphology of pores follows wedge-type cracks interconnected to each other at grain boundaries. Here, interconnected porosity with small particle necks dominate. The observations made from the pinned grain boundaries by pores are as follows:

1. The segment of the grain boundary closest to the pore is straight having no curvature.
2. The point where the grain boundary is pinned at the pore's surface is between two different curvatures.
3. The segment of the grain boundary that is not pinned is curved.

4. Discussion

By deploying Gibbsian interfacial thermodynamics without ignoring effects of surface curvature, and through experimental results, we hope to demonstrate that grain boundary detachment from pores is only possible with pore spherodizing, which results from pore rounding owing to surface diffusion.

The micrographs seen in Fig.2 to Fig.4 clearly indicate that the alloying, heat treatment, time and temperature have a significant influence on the sintering response of the material and the morphology of the pores in the sintered material.

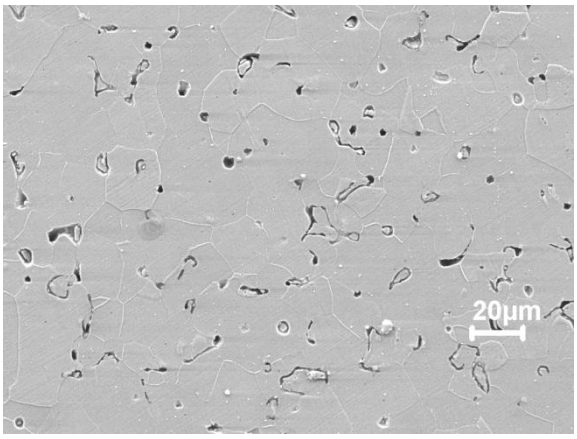

Figure 4. Optical micrograph of Sample3 decarburized at 960 C. Irregular crack-like lines at the grain boundaries and some spherical pores, as well as a spherical internal porosity are observed.

The porosity seen here is typical of most ferrous P/M materials. The analysis of the evolution of the microstructures through the use of heat treatment of Sample1 can be utilized to explain the effect of P content on the morphology of pores as reported earlier [19]. Heat treatment of the low C content in Sample1 resulted in increased pore refinement. Heat treatment resulted in higher, almost complete, dissolution of Fe_3P. This provides a higher P content at the grain boundaries which resulted in pore rounding.

Heat treatment promotes neck growth and solid phase sintering leading to change in pore morphology. Fig.1 shows how pores are more rounded. It can be seen from Fig.1 through Fig.4 how pores are located at grain boundaries and increase in size relatively. Looking at the micrographs, one can find many examples of bent

boundaries in cases where equilibrium is not attained, and planar or straight grain boundaries when equilibrium is attained. When the pore's two parts, the trailing and the advanced part, have two different radii of curvature the slope of the two parts at the point of intersection with the grain boundary will be different as seen in Fig.5. The grain boundary is also a straight line.

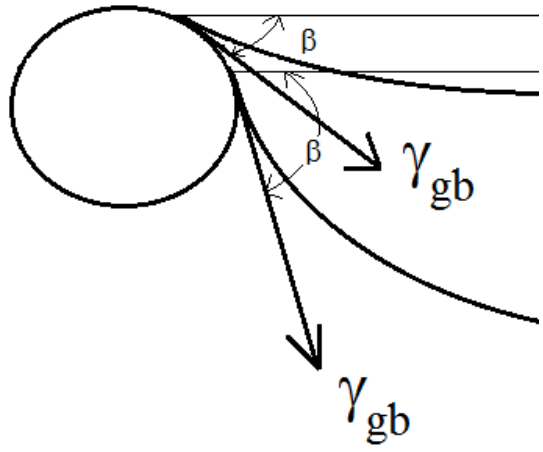

Figure 5. Schematic representation of a migrating grain boundary showing geometrically, a decreasing β value.

At equilibrium with no grain migration, there should be a balance of forces at the junction between the pore surface and the grain boundary. This is governed by the equation:

$$\gamma_{gb}\cos\beta = \gamma_{sv2}\cos\theta_2 - \gamma_{sv1}\cos\theta_1 \tag{3}$$

, while taking the total derivative of γ_{gb} to be:

$$d\gamma_{gb} = \frac{\partial\gamma_{gb}}{\partial\gamma_{sv1}}d\gamma_{sv1} + \frac{\partial\gamma_{gb}}{\partial\gamma_{sv2}}d\gamma_{sv2} + \frac{\partial\gamma_{gb}}{\partial\theta_1}d\theta_1 + \frac{\partial\gamma_{gb}}{\partial\theta_2}d\theta_2 + \frac{\partial\gamma_{gb}}{\partial\beta}d\beta \tag{4}$$

, and the total derivative $d\gamma_{gb}$ as:

$$d\gamma_{gb} = -\frac{\cos\theta_1}{\cos\beta}d\gamma_{sv1} + \gamma_{sv1}\frac{\sin\theta_1}{\cos\beta}d\theta_1 + \frac{\cos\theta_2}{\cos\beta}d\gamma_{sv2} - \gamma_{sv2}\frac{\sin\theta_2}{\cos\beta}d\theta_2 + \gamma_{gb}\tan\beta d\beta \tag{5}$$

Knowing that the curvature k is the derivative of the tangent angle θ with respect to the arc length [22], the curvature at that point is:

$$\frac{d\theta}{ds} = \frac{dT}{ds} = k \quad \text{and} \quad \frac{d\beta}{ds_{gb}} = k_{gb} \tag{6}$$

Using the definition of the curvature in eq.(5) and dividing by ds we obtain:

$$\frac{d\gamma_{gb}}{ds} = -\frac{\cos\theta_1}{\cos\beta}\frac{d\gamma_{sv1}}{ds} + \frac{\cos\theta_2}{\cos\beta}\frac{d\gamma_{sv2}}{ds} + \gamma_{sv1}\frac{\sin\theta_1}{\cos\beta}k_1 - \gamma_{sv2}\frac{\sin\theta_2}{\cos\beta}k_2 + \gamma_{gb}\tan\beta k_{gb}\frac{ds_{gb}}{ds} \tag{7}$$

The presence of the derivative of the grain boundary energy and the free surface indicates that both the boundary energy and the surface energy vary with the normal of the pore and the normal to the grain boundary at the point of intersection. This is a torque term per unit area of the pore. The tangential component of this equation acts to minimize the surface area, while the normal component rotates the interface towards an orientation with a lower interfacial area.

At minimum energy, the surface tension of the intersection must be in mechanical equilibrium, satisfying the following Herring torque relation [23]:

$$\sum_{i=1}^{3}\left(\gamma_i\hat{t}_i + \frac{\partial\gamma_i}{\partial t_i}\hat{n}_i\right) = 0 \tag{8}$$

The summation of the torque terms should be zero to satisfy mechanical equilibrium. The junction between a pore and two grains is considered to be a poly-phase junction. Thus, the angle between two inter-phase boundaries is the dihedral angle. By examining the micrographs, in particular the junctions between pores and grain boundaries, it is evident that the two grain-pore junctions do not meet at 120°. This confirms that the interfacial energy and the grain boundary energy is not constant with the orientation of the interface and the grain boundary. This means that the normal term in eq.(8) should be considered. The angle varies according to the relative orientation of the grains at the junction.

When the specific surface free energy is isotropic, the resulting pore surface defines a sphere. Thus leading to the conclusion that $\gamma 1=\gamma 2$ and $d\gamma=0$. This means that here, there is no need for a grain boundary between the two points.

For the present discussion we may consider that only the energy of the pore surface remains unchanged during the growth of the grain. Thus, forcing $\gamma_{sv1}=\gamma_{sv2}$ and $\theta_1+\theta_2=180$ leading to $\sin\theta_1=\sin\theta_2$ and $\cos\theta_1=-\cos\theta_2$. In addition, from the experimental observation of the pore's equal curvature at the point of conjunction, at the trailing and advanced parts, we set $k_1=k_2$. Substituting these conditions into eq.(5) yields:

$$\frac{d\gamma_{gb}}{ds} = +\gamma_{gb}\tan\beta k_{gb}\frac{ds_{gb}}{ds} \tag{9}$$

,and using the definition of the curvature again, we find:

$$\frac{d\gamma_{gb}}{ds} = \gamma_{gb} \tan\beta \frac{d\beta}{ds} \quad (10)$$

This additional force on the grain boundary can be interpreted physically as producing a torque on the moving grain boundary that changes the moving grain boundary direction so as to follow the periphery of the pore surface. The force that produces this torque must act perpendicularly to the grain boundary's propagation direction. The Herring torque is produced by a physical force associated with the grain boundary energy γ_{gb}, which is generally anisotropic. This force acts perpendicularly to each grain boundary segment at the junction of the grain boundaries and pores.

Pore-drag reduces the grain boundary mobility by applying a pinning pressure on grain boundaries. In order for grain growth to be inhibited, the grain boundaries must become immobile requiring the drag pressure to be larger than the driving pressure, hence:

$$P_{drag} > P_{growth} \quad (11)$$

From all the experimental observations of pores, the grain boundary is always pinned where there is a difference in curvature between the trailing part and the advanced part of the pore at the point of conjunction. Each point of the grain boundary curve migrates in the direction of the normal vector to the curve. The driving force acting on the grain boundary is due to the grain boundary curvature, Here, the change in grain boundary energy is γK dK and the pressure on a boundary is given by the Young–Laplace equation [24]:

$$P_{gb} = \gamma_{gb} k_{gb} \quad (12)$$

, where k_{gb} is the average curvature of the grain boundary. The only fronts of the grain boundary that do not move are straight line segments with $k_{gb}=0$. Also, the total derivative of the pressure acting on the grain boundary is defined as:

$$dP_{gb} = \gamma_{gb} dk_{gb} + k_{gb} d\gamma_{gb} \quad (13)$$

Dividing by ds and using eq.(10) yields:

$$\frac{dP_{gb}}{ds} = \gamma_{gb} \frac{dk_{gb}}{ds} + \gamma_{gb} \tan\beta \frac{d\beta}{ds} \quad (14)$$

Moving along the pore surface by ds from the trailing to the advance part of the pore, the pressure will be:

$$P_{gb} + \frac{dP}{ds} ds = \gamma_{gb} k_{gb} + \gamma_{gb} \tan\beta \frac{d\beta}{ds} \quad (15)$$

By examining Fig.5 one can see that geometrically $d\beta/ds \leq 0$ thus the second term on the right will decrease the pressure. Mathematically, the tangent on both sides of the grain boundary at the point of intersection is the same. This means that the first derivative does not change when crossing the point of intersection from the trailing to the advance part of the pore, which causes the pressure to decrease.

In contrast, if the slope is not the same at the point of intersection where the slope is discontinuous, is called a "cusp". Here, the grain boundary's curvature will become zero and the migrating pressure at the intersection point becomes zero. The pinning point on the pore's surface will acquire a zero pressure on the grain boundary. This point will have a zero curvature. It is a point where the curvature vanishes but does not change sign in mathematical terms. This is called an undulation point.

As illustrated by Fig.6 the intersection points are like a corners or cusps. Thus, they are local extrema points and the points of intersection are critical points. Such a critical point is the end point of the trailing part of the pore at which dk_{gb}/ds and $d\gamma_{gb}/ds$ do not exist. Thus, there will be a jump in the pressure across from the trailing part to the advance part. The intersection point jumps from the trailing part to the advance part and this jump makes the function discontinuous and pins the grain boundary.

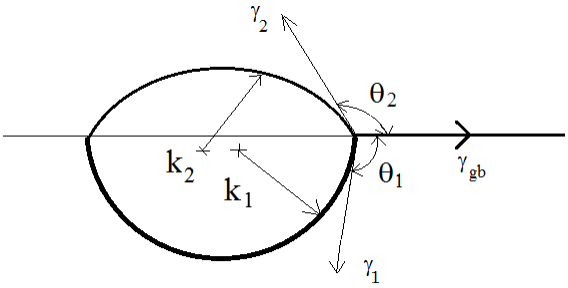

Figure 6. A schematic showing a pinned grain boundary by a pore. Here β=0.

The velocity of the Grain boundary of a growing grain is related to the driving pressure of grain growth. As described by Rollett *et al.* [25], as well as by Gottstein and Shvindlerman [26], the grain boundary velocity and pressure during primary recrystallization can be represented as:

$$v_b = M_b P \quad (16)$$

The point of intersection moving along the periphery of the pore according to eq.(14) will have a lower pressure compared to the rest of the grain boundary points. This means that the velocity of the intersection point is slower than the rest of the grain boundary. When the intersection point reaches a point on the periphery of the pore's surface having a discontinuity in β or a sudden change in curvature, it will acquire a zero velocity according to eq.(16) thus the rest of the grain boundary will catch up with the intersection point and it will plan out.

From all the observations made on pores at the points of conjunction, it can be concluded that where the grain boundary is pinned its intersection point is straight. In this work, we propose that by considering the 2-D cross section seen in Fig.7 the point of intersection between the grain boundary and the pore will migrate on the pore's periphery ahead of the rest of the grain boundary so as to keep the curvature of the migrating grain boundary convexly curved. Local equilibrium is governed by the balance between the free energy to bow the grain boundary and the free energy to bend the angle of intersection of the grain boundary. Once the intersection point reach a stage where there are two different curvature values, the intersection point will stagnate and the rest of the grain boundary will follow.

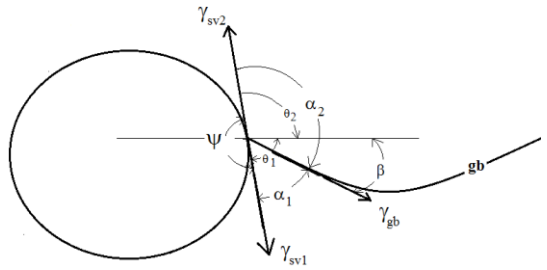

Figure7. Schematic illustration of an unpinned grain boundary for a solid-pore.

5. Conclusions

The pore surface consists of circular arcs in two dimensions and spherical caps in three dimensions. The grain boundary migrates as long as the curvature of the circular segment is constant; however, as the migrating grain boundary meets a junction of two arcs with different curvatures, or a junction of one arc and a straight segment, or a junction of two linear segments, it will be pinned at the pore surface and the grain boundary will attain a zero curvature. The morphology of pinned pores on grain boundaries is characterized by a lenticular shape with different curvatures at the intersection point from the trailing part and from the advanced part.

Consequently, detachment from pores is only possible with pore spherodizing, which results from pore rounding due to surface diffusion.

References

[1] Kang S-JL. Sintering: Densification, Grain growth and Microstructure. Amsterdam: Elsevier: 2005.

[2] B. Selvam, A.P. Singh, “Densification and deformation behavior of sintered P/M Zinc-Zinc oxide composite during cold upsetting”. Jordan Journal of Mechanical and Industrial Engineering, Vol. 5 (2011), No. 5, 447-450.

[3] R.L. Coble, "Sintering crystalline solids. I. Intermediate and final state diffusion models". Journal of applied physics, Vol. 32 (1961), No. 5, 787-792.

[4] T.O. Saetre, N. Ryum, O. Hunderi, "The effect of grain boundary edges on grain growth and grain growth stagnation". Materials Science and Engineering: A, 108 (1989), 33-36.

[5] R. Dannenberg, E. Stach, J.R. Groza, "Phenomenological description of grain growth stagnation for nanocrystalline films and powders". Journal of Materials Research, Vol. 16 (2001), No. 04, 1090-1095.

[6] L. Bourgeois, Ph. Dehaudt, C. Lemaignan, J. P. Fredric, "Pore migration in UO 2 and grain growth kinetics". Journal of nuclear materials, Vol. 295 (2001), No. 1, 73-82.

[7] B.R. Patterson, Y. Liu, J. Griffin, "Degree of pore-grain boundary contact during sintering". Metallurgical Transactions A, Vol. 21 (1990), No. 8, 2137-2139.

[8] Barsoum M.W.: Fundamentals of ceramics. CRC Press: 2002.

[9] Castro R., van Benthem K.: Sintering: Mechanisms of Convention Nanodensification and Field Assisted Processes. Vol. 35. Springer: 2013.

[10] H.C. Pavanati, A.M. Maliska, A.N. Klein, J.L.R. Muzart, "Comparative study of porosity and pores morphology of unalloyed iron sintered in furnace and plasma reactor", Materials Research, Vol. 10 (2007), No. 1, 87-93.

[11] W.Y. Shih, W. Shih, I.A. Aksay, "Elimination of an isolated pore: Effect of grain size". Journal of materials research, Vol. 10 (1995), No. 04, 1000-1015.

[12] R.T. DeHoff, "Engineering of microstructures". Materials Research, Vol. 2 (1999), No. 3, 111-126.

[13] A.L. Stuijts, "Synthesis of Materials from Powders by Sintering". Annual Review of Materials Science, Vol. 3 (1973), No. 1, 363-395.

[14] F.A. Nichols, "Further comments on the theory of grain growth in porous compacts". Journal of the American Ceramic Society, Vol. 51 (1968), No. 8, 468-468.

[15] R.J. Brook, "Controlled grain growth". Treatise on materials science and technology, Vol. 9 (1976), 331-364.

[16] H.H. Yu, Z. Suo, “An axisymmetric model of pore-grain boundary separation”. Journal of the Mechanics and Physics of Solids, Vol. 47 (1999), No. 5, 1131-1155.

[17] M. Hillert, "On the theory of normal and abnormal grain growth". Acta metallurgica, Vol. 13 (1965), No. 3, 227-238.

[18] Y.C. Zhu, J.H. Mao, F.T. Tan, X.L. Qiao, "A role of low energy grain boundaries in the abnormal grain growth in Fe-3% Si alloy". Applied Mechanics and Materials, Vol. 127 (2012), 89-94.

[19] W. Khraisat, "Graphite pore filling and surface blistering of sintered Fe–C–Si". Powder Metallurgy, Vol. 55 (2012), No. 3, 242-247.

[20] A. Molinari, G. Straffelini, V. Fontanari, R. Canteri, “Sintering and microstructure of phosphorus Steels”. Powder Metallurgy, Vol. 35 (1992), No. 4, 285-291.

[21] S. Channappagoudar, K. Aithal, N. Sannayallappa, V. Desai, P.G. Mukunda, "The Influence of the Addition of 4.5 wt.% of Copper on wear properties of Al-12Si eutectic alloy". Jordan Journal of Mechanical and Industrial Engineering, Vol. 9 (2015), No. 3.

[22] Sapidis NS. Designing fair curves and surfaces: shape quality in geometric modeling and computer-aided design. Society for Industrial and Applied Mathematics: 1994.

[23] Herring C. Surface tension as a motivation for sintering. Fundamental Contributions to the Continuum Theory of Evolving Phase Interfaces in Solids. 33-69. Berlin Heidelberg: Springer: 1999.

[24] Laplace PS. Suppl´ement au dixi`eme livre du Trait´e de M´ecanique C´eleste: Sur l’action capillaire. Edité par ReInk. De L’Imprimerie de Crapelet: 1805.

[25] A.D. Rollett, G. Gottstein, L.S. Shvindlerman, D.A. Molodov, “Grain boundary mobility–a brief review”. Zeitschrift für Metallkunde, Vol. 95 (2004), No. 4, 226-229.

[26] Gottstein G, Shvindlerman LS. Grain boundary migration in metals: thermodynamics, kinetics, applications. 2nd ed. CRC press: 2010.